Molecular Motion in Crystalline Naphthalene: Analysis of Multi-Temperature X-Ray and Neutron Diffraction Data

Silvia C. Capelli

European Synchrotron Radiation Facility, BP220, F-38043 Grenoble, France

Alberto Albinati

Department of Structural Chemistry, University of Milan, Via G. Venezian 21, I-20133 Milan, Italy

Sax A. Mason

Institut Laue-Langevin, BP156, F-38042 Grenoble, France

Bertram T. M. Willis*

Chemistry Research Laboratory, University of Oxford, Mansfield Road, Oxford, OX1 3TA, United Kingdom

Received: May 15, 2006; In Final Form: July 26, 2006

Single crystals of h_8-naphthalene have been examined by both X-ray and neutron diffraction over a range of temperatures from 5 to 295 K. The aim of this case study was to measure the anisotropic displacement parameters (ADPs) of carbons and hydrogens and to interpret them using the model of thermal motion proposed by Bürgi and Capelli (*Acta Cryst.* **2000**, *A56*, 403). The traditional rigid-body analysis expresses the low-frequency motions in terms of molecular translations and librations only, whereas the Bürgi−Capelli treatment also includes the high-frequency internal modes. We show that a considerable improvement occurs by representing the internal modes by a single second-rank tensor and that a further improvement follows by including a Grüneisen parameter to account for volume thermal expansion. By applying the treatment to multi-temperature diffraction data, there is a considerable reduction in the ratio of number of adjustable parameters/number of independent observations.

Introduction

Atomic displacement parameters (ADPs) are routinely derived in crystal-structure analysis. They relate to the mean-square displacements of the atoms from their average positions in the crystal. For molecular crystals, Cruickshank showed that these quantities can be interpreted in terms of the rigid-body vibrations of the molecule and allow the calculation of its thermodynamic properties.[1−3] Cruickshank's analysis was subsequently extended by Schomaker and Trueblood[4] who formulated the so-called TLS model, which is in wide use today. This model yields three second-rank tensors that are associated with the external modes of vibration: the molecular translation tensor (T), the libration tensor (L), and the tensor S representing correlation between the translational and librational motion.

The rigid-body TLS model has significant shortcomings: the trace of S cannot be determined because it depends on the unknown correlation of the displacement amplitudes and it takes no account of intramolecular vibrations. These limitations were addressed by Bürgi and Capelli,[5] who proposed an alternative method of analyzing the ADPs. Their model describes the temperature evolution of the ADPs, which are partitioned into temperature-dependent and temperature-independent portions, the former including molecular librations and translations and the latter including molecular deformations. In their formalism, the atomic mean square displacement matrix Σ^X, of which the 3×3 diagonal blocks are the experimental ADPs, is expressed in terms of normal-mode frequencies and eigenvectors:

$$\Sigma^X(T) = \mathbf{AgV}\boldsymbol{\delta}(T)\mathbf{V}^T\mathbf{g}^T\mathbf{A}^T + \boldsymbol{\epsilon} \qquad (1)$$

Where **A** is the transformation matrix from atomic to normal mode coordinates, **g** is the mass correction matrix, **V** is the eigenvector matrix, $\boldsymbol{\epsilon}$ is the symmetric matrix of the mean-square displacements arising from the high-frequency intramolecular vibrations, and $\boldsymbol{\delta}(T)$ is the diagonal matrix of the temperature-dependent mean-square normal mode displacements. For each normal mode j, with associated frequency ω_j, the mean-square amplitude is given by:

$$\delta_j(T) = (h/2\omega_j)\coth(h\omega_j/2k_BT) \qquad (2)$$

This formalism results in an internally consistent physical model that allows us to describe the ADPs in a wide temperature range with a small and unique set of parameters. When only the three rigid-body librations and the three rigid-body translations are considered in the model of motion, the first part of eq 1 can be easily rewritten in the well-known Schomaker and Trueblood formalism:

$$\Sigma^X = \mathbf{A}\begin{pmatrix}\mathbf{T} & \mathbf{S}\\ \mathbf{S}^T & \mathbf{L}\end{pmatrix}\mathbf{A}^T + \boldsymbol{\epsilon} \qquad (3)$$

* To whom correspondence should be addressed. E-mail: bertram.willis@chem.ox.ac.uk; Tel: (+44) 1865 557601; Fax: (+44) 1865 285021.

10.1021/jp062953a CCC: $33.50
Published on Web 09/27/2006

Provided diffraction data are available at various temperatures (preferably in both the low-temperature quantum and the high-temperature classical regimes), the elements of V, the frequencies of the normal modes ω_j and the 3×3 diagonal blocks of the ϵ tensor can be obtained by least-squares fitting from the experimental ADPs.

To account for the effects of anharmonicity resulting in thermal expansion and variation with temperature of the normal-mode frequencies, a Grüneisen parameter[6] $\gamma_G(j)$ for each normal mode j has been introduced in the model:

$$\gamma_G(j) = -\frac{V_0}{\omega_0}\cdot\frac{\Delta\omega}{\Delta V} \quad (4)$$

In this way, a direct dependence of the effective normal-mode frequency on the temperature is achieved:

$$\omega_{\text{eff}}(j,T) = \omega_0(j)[1 - \gamma_G(j)\,\Delta V/V_0\,\chi T] = \omega_0(j)[1 - \gamma_G(j)\,\chi T] \quad (5)$$

where ω_0 and ω_{eff} are respectively the harmonic frequency and the effective anharmonic frequency of the jth normal mode and $\chi = \Delta V/V_0$ is the coefficient of thermal expansion.

Naphthalene is one of the first molecules to which Cruickshank applied his theory of the rigid-body vibrations of a molecule in a crystal. From the anisotropic displacement parameters refined from X-ray diffraction data, he calculated the amplitude of the translational vibrations of the center of mass and the angular oscillations about the inertial axes of the molecule. These values allowed him also to calculate the mean frequencies for the optic branches of lattice vibrations.[1−3] In his work, Cruickshank also predicted the temperature dependence of translational and librational motions in naphthalene. Later, Pawley and Yeats[7] used the formalism developed by Cruickshank to refine the structure of perdeutero-naphthalene from single-crystal neutron diffraction data in the rigid-body thermal motion model and derived ADPs from the refined **T** and **L** tensors. Cruickshank's predictions on temperature-dependence of molecular motion in naphthalene were tested experimentally by Brock and Dunitz[8] on single-crystal X-ray diffraction data collected between 92 and 240 K using the Schomaker and Trueblood TLS formalism and showed some limitations in explaining the low-temperature data, suggesting that an appropriate correction for anharmonicity had to be applied to the Cruickshank treatment. Baharie and Pawley[9] also tried to understand the effect of anharmonicity in crystalline perdeutero-naphthalene using neutron diffraction from a powder sample in a temperature range from 5 to 293 K, and they showed that reasonable **T** and **L** tensors could be obtained by powder diffraction data, provided that an adequate treatment of the background was made. Recently, a new attempt to analyze the Brock and Dunitz diffraction data with the Bürgi−Capelli method has been made,[10] but the lack of diffraction data in the low-temperature quantum regime was a limitation in determining the thermal motion of naphthalene in the crystal. Oddershede and Larsen,[11] who investigated the electron density of naphthalene in attempting to deconvolute the thermal motion from the diffraction data, have collected new X-ray data in the classical regime (>100 K). Moreover, naphthalene and perdeutero-naphthalene have been subjected to extensive studies by many other techniques, ranging from IR and Raman studies[12−27] to the determination of the phonon frequencies and density of states from inelastic neutron scattering,[28−36] together with lattice-dynamical,[37−41] molecular dynamics,[42,43] and theoretical calculations.[44−48] Studies on nonrigidity,[49,50] anharmonicity,[51,52] and pressure dependence of lattice modes[53,54] have also been performed.

In this paper, we describe the measurement of both X-ray and neutron diffraction data on single-crystal h_8-naphthalene in both the quantum and the classical regimes (i.e., between 5 and 293 K) and the derivation of the molecular motion in the solid from the temperature-dependence of the experimental ADPs. We then compare the results obtained by using the TLS and the Bürgi−Capelli treatments with the literature data.

Experimental Methods

Synchrotron X-ray Data. X-ray intensity data for a single crystal of h_8-naphthalene grown from ethanol solution (size $0.15 \times 0.1 \times 0.1$ mm^3) were collected with a Bruker-SMART-CCD detector at the ID11 beamline of the European Synchrotron Radiation Facility (ESRF), Grenoble, at 32 keV ($\lambda = 0.38745(2)$ Å) and at 10, 30, 60, 90, 120, 150, 180, and 220 K. The 10, 30, and 60 K data were collected using an Oxford-diffraction Helijet open-cycle helium cryostream, whereas the data from 90 to 220 K were obtained using an Oxford-cryosystem open-cycle nitrogen cryostream. Due to icing problems at the end of the 60 K data collection, the crystal cracked and a new crystal of comparable size had to be used for the 90−220 K measurements.

A sample to detector distance of 8.223 cm gave a resolution at the edge of the CCD detector of 0.57 Å ($\sin\theta/\lambda = 0.88$ Å^{-1}). Three series of 450 frames were collected with a ϕ-scan and a rotation width of 0.4° with exposure time of 1 s at fixed ω position ($\omega = -155, -110, -55°$) to better sample reciprocal space (6 h total collection time per temperature). For the three helium-temperature datasets, only one series of 450 frames could be used for integration, due to alignment problem of the Helijet head that produced ice on the crystal in the −110 and −55° ω positions. Cell dimensions and space group were determined with the Bruker-SMART software[55] from all reflections with $I/\sigma(I) > 50$ in the first 450 images of each data collection. On average, a total of ~5000 and ~13 000 reflections per data set were integrated with the program SAINT[55] respectively for the helium and nitrogen temperatures, ~1900 of which were unique (R_{int} in the range 0.0225−0.0402), giving an average completeness of the datasets of ~93% for the three lowest temperatures and ~96% for the others. Because of the short wavelength used in the experiment, no absorption correction was made. Initial models of the structures were obtained by direct methods and refined by full matrix least-squares on F^2 using SHELX97.[56] All carbon atoms were refined anisotropically. Hydrogen atoms were located in the difference Fourier map and refined freely.

Neutron Data. Neutron data sets were collected on a single crystal of h_8-naphthalene grown from ethanol and sealed in a quartz tube to minimize sublimation (size $4 \times 2 \times 1$ mm^3). Measurements were made on the four-circle diffractometer D9 at the Institut Laue-Langevin, Grenoble, at a wavelength of 0.840 Å in a 2 K four-circle cryo-refrigerator at six temperatures: 5, 30, 80, 150, 220, and 295 K. At 295 K, the reflection intensities were too weak for recording above $2\theta = 60°$, but measurements at somewhat higher angles were possible at the other temperatures. For all temperatures, at least 600 unique reflections were measured, each after averaging two or more symmetry-equivalent reflections (R_{int} in the range 0.0121−0.0256). No absorption correction was applied. Standard software was used to analyze the data and determine the lattice parameters. The same initial models of the structures used in the refinement of the X-ray data were refined by full matrix least-squares on F^2 using SHELX97.[56] All hydrogen atoms were

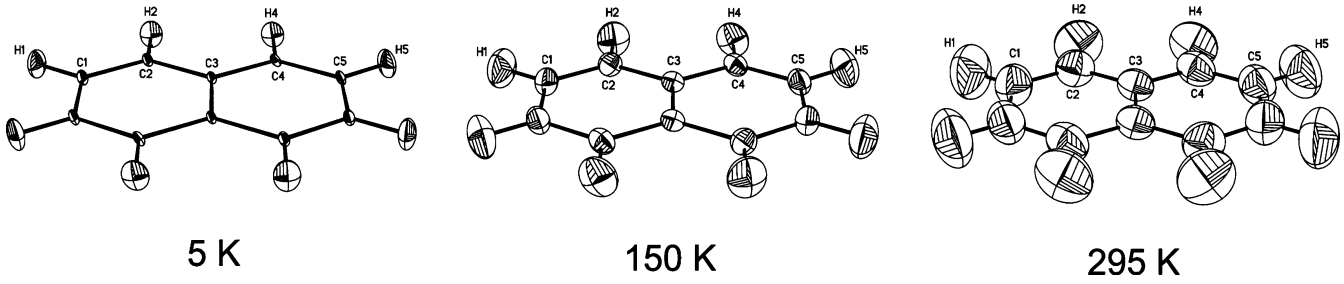

Figure 1. ORTEP[57] thermal ellipsoids of the carbon and hydrogen atoms, as calculated from neutron diffraction data at three temperatures.

TABLE 1: Normal-Mode Frequencies: X-ray Synchrotron Data at 10, 30, 60, 90, 120, 150, 180, and 220 K

model	eigenvector	frequency (cm^{-1})	ϵ (carbon)	Grüneisen γ	GOF	R (%)
TLS	$0.90L_x$, $0.09L_y$, $0.01L_z$	104(3)			2.98	5.1
	$0.09L_x$, $0.91L_y$	70.9(8)				
	$0.01L_x$, $0.99L_z$	51.7(3)				
	$0.96T_x$, $0.04T_y$	39.6(1)				
	$0.03T_x$, $0.96T_y$, $0.01T_z$	44.0(2)				
	$0.01T_y$, $0.99T_z$	46.3(4)				
TLS, ϵ	$0.90L_x$, $0.09L_y$, $0.01L_z$	103(3)	−6(1) 0(0) 0(0)		2.70	4.6
	$0.09L_x$, $0.91L_y$	70.6(7)	−7(1) 0(0)			
	$0.01L_x$, $0.99L_z$	51.4(3)	−3(1)			
	$0.96T_x$, $0.04T_y$	38.8(1)				
	$0.04T_x$, $0.94T_y$, $0.02T_z$	44.0(2)				
	$0.01T_y$, $0.99T_z$	45.9(4)				
TLS, ϵ, γ	$0.90L_x$, $0.09L_y$, $0.01L_z$	109(2)	2(1) 0(0) 0(0)	2.3(1)	1.84	3.0
	$0.09L_x$, $0.91L_y$	74.1(6)	1(1) 1(0)			
	$0.01L_x$, $0.99L_z$	53.8(2)	5(1)			
	$0.96T_x$, $0.04T_y$	41.9(2)				
	$0.04T_x$, $0.95T_y$, $0.01T_z$	47.7(2)				
	$0.01T_y$, $0.99T_z$	50.0(3)				

located in the difference Fourier map and all atoms were refined anisotropically.[77]

Modeling of Thermal Motion. ORTEP[57] drawings of the thermal ellipsoids obtained at three temperatures from neutron diffraction data are shown in Figure 1. They show clearly the presence of both translational and librational motion of the entire molecule.

In the temperature range 5−295 K, naphthalene crystallizes in space group $P2_1/a$ with two molecules per unit cell. (The nonstandard $P2_1/a$ space group setting has been retained for consistency with previous work.) The crystal symmetry is C_{2h}^5 and factor group analysis shows that there are 12 lattice modes, 6 Raman-active librations (3 with A_g and 3 with B_g symmetry), 3 IR-active translations (2 with A_u and 1 with B_u symmetry), and 3 acoustic vibrations not observable at the origin of the Brillouin zone. In the ADP-analysis presented in this work, we have used the mean field approximation, i.e., we treated the case of a single molecule moving in the mean field of its surrounding crystalline environment, and so we condidered only 6 external modes.

Three different models of thermal motion have been used in fitting the observed ADPs. The first uses the usual degrees of freedom of the rigid-body model (TLS) with three translational frequencies and the associated eigenvectors each with three components T_x T_y T_z, and three librational frequencies with the corresponding eigenvectors with components L_x L_y L_z. The correlation tensor **S** is always zero for naphthalene, on account of symmetry, and so the TLS model is the same as the original TL model of Cruickshank. In the second model (TLS, ϵ), a constant symmetric 3×3 block diagonal matrix ϵ is added at all temperatures, representing the temperature-independent correction term for the intramolecular vibration of the carbon and hydrogen atoms (the blocks for the hydrogen atoms have been introduced only in the analysis of the neutron data). In the third model (TLS, ϵ, γ), a single Grüneisen parameter γ is included for all six external modes to account for the influence of thermal expansion. Note that these models are less sophisticated (i.e., contain fewer adjustable parameters) than those used by Bürgi et al.[10] in the analysis of the Brock and Dunitz X-ray data,[8] but our aim is to examine whether the addition of a rather limited number of extra parameters is justified.

All the ADP sets were analyzed in a molecular coordinate system for which the *x*-axis corresponds to the long axis of the molecule, the *y*-axis is orthogonal to the *x*-axis and lies in the molecular plane, and the *z*-axis completes the right-handed orthogonal set. The blocks of the ϵ tensor are expressed in a local coordinate system having the 11-direction along the C−C−C exocyclic bisectors for the carbon atoms, or along the C−H bond for the H atoms, the 22-direction orthogonal to the 11-direction in the molecular plane and the 33-direction in the out-of-plane direction.

Results

1. Molecular Motion in the Crystal. *1.1. X-ray Results.* The results from the analysis of the ADPs obtained by synchrotron X-ray measurements at eight different temperatures in the range 10−220 K are illustrated in Table 1. The normal-mode frequencies, the eigenvector components, the Grüneisen parameter, and the elements of the ϵ tensors were obtained by least-squares fitting against the observed ADPs, using the program NKA.[58]

In Table 1, we see that the eigenvectors and frequencies are little changed from one model to another. In the (TLS,ϵ) model, the extra tensor ϵ accounting for the high-frequency modes has negative components, indicating the presence of anharmonicity

TABLE 2: Normal-Mode Frequencies: X-ray Laboratory Data at 100, 135, 170, and 205 K

model	eigenvector	frequency (cm^{-1})	ϵ (carbon)			Grüneisen γ	GOF	R (%)
TLS	$0.90L_x$, $0.09L_y$, $0.01L_z$	103(3)					15.7	3.2
	$0.09L_x$, $0.91L_y$	69.7(6)						
	$0.01L_x$, $0.99L_z$	52.8(3)						
	$0.92T_x$, $0.07T_y$, $0.01T_z$	40.5(1)						
	$0.07T_x$, $0.87T_y$, $0.06T_z$	45.8(2)						
	$0.07T_y$, $0.93T_z$	45.1(3)						
TLS, ϵ	$0.90L_x$, $0.09L_y$, $0.01L_z$	103(2)	−16(1)	0(0)	0(0)		11.7	2.4
	$0.09L_x$, $0.91L_y$	69.7(5)		−21(2)	0(0)			
	$0.01L_x$, $0.99L_z$	51.9(3)			−2(2)			
	$0.94T_x$, $0.06T_y$	38.3(2)						
	$0.05T_x$, $0.94T_y$, $0.01T_z$	43.1(3)						
	T_z	44.7(4)						
TLS, ϵ, γ	$0.91L_x$, $0.08L_y$, $0.01L_z$	108(2)	11(2)	0(0)	0(0)	2.9(2)	8.4	1.7
	$0.09L_x$, $0.91L_y$	73.0(4)		7(2)	0(0)			
	L_z	54.7(3)			24(2)			
	$0.94T_x$, $0.06T_y$	43.9(4)						
	$0.05T_x$, $0.94T_y$, $0.01T_z$	50.5(6)						
	T_z	52.8(7)						

TABLE 3: Normal-Mode Frequencies: Neutron Data at 5, 30, 80, 150, 220, and 295 K

model	eigenvector	frequency (cm^{-1})	ϵ (carbon)			ϵ (hydrogen)			Grüneisen γ	GOF	R (%)
TLS	$0.74L_x$, $0.26L_y$	63(2)								6.1	22.2
	$0.26L_x$, $0.74L_y$	53(1)									
	L_z	44(1)									
	$0.93T_x$, $0.06T_y$, $0.01T_z$	35.5(4)									
	$0.06T_x$, $0.92T_y$, $0.02T_z$	40.2(8)									
	$0.02T_y$, $0.01T_y$,$0.97T_z$	52(2)									
TLS, ϵ1	$0.87L_x$, $0.13L_y$	91(4)				57(6)	1(4)	6(5)		3.4	12.2
	$0.13L_x$, $0.87L_y$	64(1)					130(6)	−9(5)			
	L_z	49(1)						210(7)			
	$0.88T_x$, $0.09T_y$, $0.03T_z$	35.6(2)									
	$0.05T_x$, $0.84T_y$, $0.11T_z$	39.2(4)									
	$0.07T_y$, $0.07T_y$,$0.86T_z$	43(1)									
TLS, ϵ2	$0.87L_x$, $0.13L_y$	91(3)	6(3)	2(2)	6(2)	58(6)	1(4)	6(4)		3.3	11.8
	$0.13L_x$, $0.87L_y$	64(1)		−2(3)	−9(2)		128(6)	−4(5)			
	L_z	48(1)			2(2)			211(7)			
	$0.89T_x$, $0.10T_y$, $0.01T_z$	35.9(3)									
	$0.07T_x$, $0.84T_y$, $0.09T_z$	39.9(5)									
	$0.04T_y$, $0.06T_y$,$0.90T_z$	43(1)									
TLS, ϵ, γ	$0.89L_x$, $0.11L_y$	110(2)	21(3)	2(1)	6(1)	75(3)	2(2)	6(2)	4.0(1)	1.9	6.6
	$0.11L_x$, $0.89L_y$	75.6(8)		17(1)	−10(1)		156(3)	−14(3)			
	L_z	56.7(5)			22(1)			242(4)			
	$0.90T_x$, $0.07T_y$, $0.03T_z$	43.8(3)									
	$0.09T_x$, $0.86T_y$, $0.05T_z$	49.4(5)									
	$0.01T_y$, $0.07T_y$,$0.92T_z$	53.5(6)									

in the ADPs.[59] In fact, when a Grüneisen parameter γ is included, i.e., the (TLS,ϵ,γ) model, all the components of ϵ become positive.

The outcome of an equivalent ADP analysis of the laboratory X-ray data measured by Oddershede and Larsen[11] at four temperatures between 100 and 205 K is shown in Table 2. We note that the results in Tables 1 and 2 are quite similar, despite the fewer temperatures of the laboratory X-ray data. Indeed, in terms of R factors, it appears that the laboratory results are superior to those obtained with the synchrotron, whereas according to the goodness-of-fit (GOF), the latter are preferred. The better R factor for the laboratory data could be ascribed to the better resolution of the diffraction data ($\sin\theta/\lambda = 1.16$ Å^{-1}) resulting in an improved determination of the experimental ADPs, whereas the high GOF for the same data could likely be due to the very small standard deviations on the ADPs obtained in the laboratory.

In Table 2, we observe the same progression as in Table 1: a continuous improvement of the fit with increasing complexity of the model of motion, negative elements of the ϵ tensor that become positive when anharmonicity is taken into account, values of the normal-mode frequencies within two standard deviations of those given in Table 1, and finally similar eigenvector components and values of the γ Grüneisen parameter.

1.2. Neutron Results. Table 3 refers to the neutron results from measurements on the D9 diffractometer at the Institut Laue-Langevin, Grenoble. In this case, we have employed two versions of the second model (TLS,ϵ). In (TLS,ϵ**1**), only the hydrogen contributions to the ϵ tensor are considered [Model (TLS,ϵ**1**) has been considered for consistency with the "TLS-corrected" model widely used in the neutron diffraction community], whereas in (TLS, ϵ**2**), additional contributions for the carbon atoms are introduced. Unlike the X-ray results, the frequencies are considerably altered when extra parameters are incorporated in the TLS model. These frequencies are remarkably similar for all the "enhanced" models and are comparable with those obtained by X-rays. The ϵ components for (TLS,ϵ**1**), (TLS,ϵ**2**), and (TLSϵ,γ) are all positive, and the Grüneisen γ parameter is a little larger than those obtained from X-ray data.

TABLE 4: Summary of Lattice Mode Frequencies for Naphthalene Using Various Techniques

technique	*T* (K)	translational frequencies (cm^{-1})	librational frequencies[a] (cm^{-1})	ref.
ADP-analysis on X-ray data	10−220	41.9 47.7 50.0	53.8 74.1 109	this work
ADP-analysis on neutron data	5−295	43.8 49.4 53.5	56.7 75.6 110	
rigid-body analysis on X-ray data	RT		47 62 84	3
Raman spectroscopy	RT		54 76 $109_{(S)}$	12
			45 74 $127_{(A)}$	
polarized Raman	4		69 88 120	
			56 81 141	17
	293		51 74 109	
			46 71 125	
Raman spectroscopy	2		68 89 121	21
			57 84 141	
Raman spectroscopy (d_8-naphthalene)	25		65 95 112	
			55 80 131	24
	292		45 69 100	
infrared spectroscopy	RT	53 66 98		16
far-infrared	80	66 105		18
far-infrared	4	78.6 109		20
terahertz absorption spectroscopy	RT	65		27
coherent INS (d_8-naphthalene)	6	58 78 107	64 84 112	29
			54 79 130	
coherent INS (d_8-naphthalene)	98	51 77 106	61 80 109	29
			53 78 127	
incoherent INS (d_8-naphthalene)	5	45 95	64 80 110	30
			50 70 135	
theoretical calculations (Williams' potential V)	RT	46 62 91	57 87 109	19
			47 80 105	
theoretical calculations (anharmonic potential)	RT	56 73 108	57 87 117	51
			55 84 140	

[a] (S) = symmetric mode; (A) = antisymmetric mode.

Clearly, there is a progressive improvement in the fits to the neutron data as we progress from the TLS to the TLSϵ,γ model.

1.3. Discussion. The normal mode harmonic frequencies obtained for the rigid body degrees of freedom by ADP analysis of the three different sets of diffraction data with the model (TLS,ϵ,γ) are for all practical purpose equivalent, overlapping within three standard deviations. The values for the librational modes are around 55, 74, and 109 cm^{-1}, and those for the translational modes lie in the range 42−53 cm^{-1}. Taking into account anharmonicity, i.e., calculating the effective temperature-dependent frequencies using eq 5, the values for the librational modes at the lowest temperatures (5 and 10 K) are equivalent to the harmonic ones both considering the neutron and the synchrotron X-ray data, whereas at higher temperatures, for example at 220 K where the coefficient of thermal expansion calculated from the diffraction data is very similar for the two sets of data, the frequencies change according to the Grüneisen parameter: the higher the parameter, the lower the frequency. At 220 K, the synchrotron data give effective librational frequencies of 49, 68, and 100 cm^{-1}, whereas the neutron data give values of 48, 64, and 93 cm^{-1}.

Table 4 gives a comparison of the translational and librational frequencies obtained for crystalline naphthalene using different techniques.

In their remarkable work on the Raman-active lattice modes of naphthalene, Kastler and Rousset[12] were able to identify both the symmetry and the axes of librations relative to each of the six frequencies in the spectra. At room temperature, they found that the order of the frequencies follows that of the moments of inertia of the molecule, and they were able to assign symmetric and antisymmetric librations. A few years later, Suzuki, Yokoyama, and Ito[17] studied the effect of temperature on the lattice vibrations and mean-square amplitudes of rotational oscillation, using the polarized Raman technique in the temperature range 4−293 K. They observed a high-frequency shift of the peak positions by lowering the temperature, with shifts up to ∼15 cm^{-1} when comparing the two limiting temperatures. The temperature dependence of the line shape, line width, and frequencies of Raman active phonons in naphthalene has been studied also by Bellows and Prasad[21] in the temperature range 2−290 K, confirming a frequency shift of the order of ∼12 cm^{-1} between the limiting temperatures. They observed also that the major contribution to the temperature-dependence of the phonon frequencies was due to the crystal thermal expansion.

Among the many experimental and theoretical studies found in the literature regarding the infrared spectra of crystalline naphthalene,[13−15,20,22,23,25,26,44−48] only a few of them consider the vibrational region below 400 cm^{-1} (see Table 4). This region is important in naphthalene because of the presence of out-of-plane skeletal bending occurring in the 150−200 cm^{-1} region[15] that could mix with the lattice vibrations occurring at frequencies < 150 cm^{-1}. Harada and Shimanouchi[16] observed peaks at 175 and 191 cm^{-1} and a split peak at ∼ 210 cm^{-1}, but no assumptions were made about them. Later calculations by Pawley and Cyvin[49] showed that the B_{3u} mode occurring at 176 cm^{-1} gives rise to a frequency-shift and splitting in going from the free molecule to the crystal.

A widely used experimental technique to study lattice phonons is inelastic neutron scattering. The dispersions of the low-frequency phonons have been determined by coherent inelastic neutron scattering in d_8-naphthalene at 98[29] and at 6 K[32] (the $k = 0$ frequencies are given in Table 4). In the experiment at 6 K, the authors measured the dispersion of the two lowest internal modes that appear, with two doublets at the zone center: 170/182 and 196/198 cm^{-1}, respectively, for the B_{3u} and A_u modes. A confirmation of the shift to higher

frequencies with decreasing temperature was obtained also by incoherent inelastic neutron scattering from d_8-naphthalene at 5, 80, and 296 K.[29]

Considering that the isotope effect produces a red-shift in both the Raman and IR spectra of about 10−20% when passing from h_8- to d_8-naphthalene,[22] the rigid-body frequencies obtained by ADP analysis for h_8-naphthalene are in the average range observed by other techniques. In particular, the librational frequencies obtained by ADP-analysis agree quite well, whereas the translational ones tend to be underestimated in comparison to those reported in the literature, especially in the case of the highest A_u mode, corresponding to a translation along the long molecular axis. The fact that in a theoretical calculation also the translational frequencies tend to be underestimated[19] is an indication that the mean-field approximation may not be able to treat these types of normal modes. Moreover, the effective frequencies show a temperature-dependence and a frequency-shift in line with the observations from Raman spectroscopy and inelastic neutron scattering. It is impressive to note that the librational frequencies obtained by Cruickshank in 1956 for naphthalene at room temperature, respectively 47, 62, and 84 cm^{-1}, are not far from those reported from more modern techniques and they are quite close to the frequencies calculated with the TLS model of motion. In this context, we should stress that a simple model that takes into account just the main physical parameters, such as that developed by Cruickshank, can indeed provide a satisfactory overall description of the system. However, the deeper insight gained by the present analysis justifies the increased complexity of the approach.

Anharmonicity manifests itself by the variation of line width and energy shifts with temperature or pressure. Both effects were observed in naphthalene by optical spectroscopy[24,53,54] and by inelastic neutron scattering.[34,36] In these studies, the γ Grüneisen parameters for the external phonons were determined or calculated. Dows et al.,[53] in their study of the pressure dependence of the Raman lattice modes, obtained values of the Grüneisen parameters in the range 3.6−6.3, respectively, for the highest (B_g 125 cm^{-1}) and lowest (B_g 46 cm^{-1}) frequencies. Nicol et al.[54] measured the same Raman active lattice modes as a function of temperature and pressure and reported values of γ at room temperature of 2.9 for the B_g 126 cm^{-1} frequency and of 5.1 for the 46 cm^{-1} B_g frequency. Shmelzer et al.,[34] in their incoherent inelastic scattering measurement on d_8-naphthalene, found values between 3.2 and 5.0 for the 12 branches of the external phonon dispersion curves at 100 K, whereas Sheka et al.,[36] for a similar experiment, reported values in the range 2.8−4.2. In 1987, Häfner and Kiefer[24] determined the temperature dependence of the γ Grüneisen parameter of the Raman active external modes in d_8-naphthalene, and for the temperature region 0−300 K, they calculated mean values ranging from 2.7 to 3.5. Jindal and Dlott[52] calculated mode Grüneisen coefficients for hydrostatic and uniaxial compression in h_8-naphthalene in the range 3.8−5.4 at the origin of the Brillouin zone.

In comparing our estimates of γ with those reported in the literature, we have to be cautious, in particular with the data from inelastic neutron scattering: they are not directly comparable not only because of the isotope effect but also because the variation in phonon frequencies with temperature is due to both the deformation of the unit cell with temperature and the phonon−phonon interaction. In our case, we ascribe the entire anharmonic effect to the deformation of the unit cell with temperature and we use only one parameter to describe the anharmonicity of the 12 branches of the external phonons in the entire Brillouin zone. Despite these different emphases in interpreting the Grüneisen parameter, the values obtained by ADP analysis of the three different set of diffraction data, respectively 2.3, 2.9, and 4.0, can be considered to be in broad agreement with the literature values.

The temperature-independent elements of the ϵ tensor refined from ADP analysis coming from intermolecular vibrations vary slightly according to the type of experiment. The ϵ tensor for the carbon atoms refined from synchrotron data has the smallest values whereas those refined from neutron data give larger values overall, especially for the off-diagonal elements. The laboratory X-ray data would sit exactly midway if it were not for the exception of ϵ_{33}.

The numerical values can be compared to those obtained by Bürgi et al.[10] using the same Einstein model on the X-ray data of Brock and Dunitz[8] and to ab initio calculations. First of all, one should note that in Bürgi's analysis of Brock and Dunitz data, an overall ϵ tensor, equal for all atoms and with enforced monoclinic symmetry, was used to account for systematic errors in the diffracted intensities. In this work, no overall ϵ tensor was necessary, possibly because of the low-temperature data of the neutron and synchrotron diffraction sets and of the combination of high resolution and multipole refinement for Larsen's laboratory X-ray data. The numerical values of ϵ(C) obtained from spherical refinement of the Brock and Dunitz data are larger than those obtained in this work for the neutron and synchrotron data, and those obtained from multipole refinement compare well with those derived from the refinement of the neutron data. The values for ϵ_{11} and ϵ_{22} obtained by density functional theory (DFT) calculations,[10] respectively 15 and 13 $\times$ 10^{-4} Å^2, are not too far from those obtained from neutron ADP data, whereas those obtained from synchrotron ADP data are underestimated. The DFT value of ϵ_{33}, calculated including the lowest two out-of-plane deformation frequencies (respectively 176 and 193/195 cm^{-1}, according to both theory[49] and experiment[28]), is definitely larger: 35 $\times$ 10^{-4} Å^2. Larsen's laboratory data give an ϵ tensor for the carbon atoms showing reasonable values for ϵ_{11} and ϵ_{22}, i.e., slightly smaller than the DFT calculated ones, whereas ϵ_{33} is closer to the value obtained from the neutron data. In addition, the smaller values for ϵ_{11} and ϵ_{22} and the larger value for ϵ_{33} reflect the trend of the DFT calculations.

In Figures 2 and 3, visual comparisons of the difference displacement parameters $U_{obs} - U_{calc}$ are given for the synchrotron and the neutron data sets. In the first columns, the model of motion is the Schomaker and Trueblood TLS (model TLS,ϵ1 in the case of the neutron data), and in the second column, we use the (TLS,ϵ,γ) model illustrated respectively in Tables 1 and 3 for the two sets of diffraction data. Looking at the first column, a systematic trend can be recognized both in Figures 2 and 3: the differences are mainly positive at low temperature (5−30 K), they go completely negative around 120−150 K and change again to largely positive at the upper temperature, whereas positive and negative differences in the second column are more evenly distributed, indicating a better fit of the observations.

2. Calculation of Thermodynamic Functions. The translational and librational frequencies obtained by analysis of the ADPs obtained by diffraction data can be used together with internal ab initio frequencies to calculate the molar heat capacity C_V in the solid.[61,62] Ab initio frequencies for the high-frequency normal modes of h_8-naphthalene have been calculated by DTF[26,46] and scaled quantum mechanical (SQM) methods.[26] The calculated C_V values are compared graphically in Figure 4 with

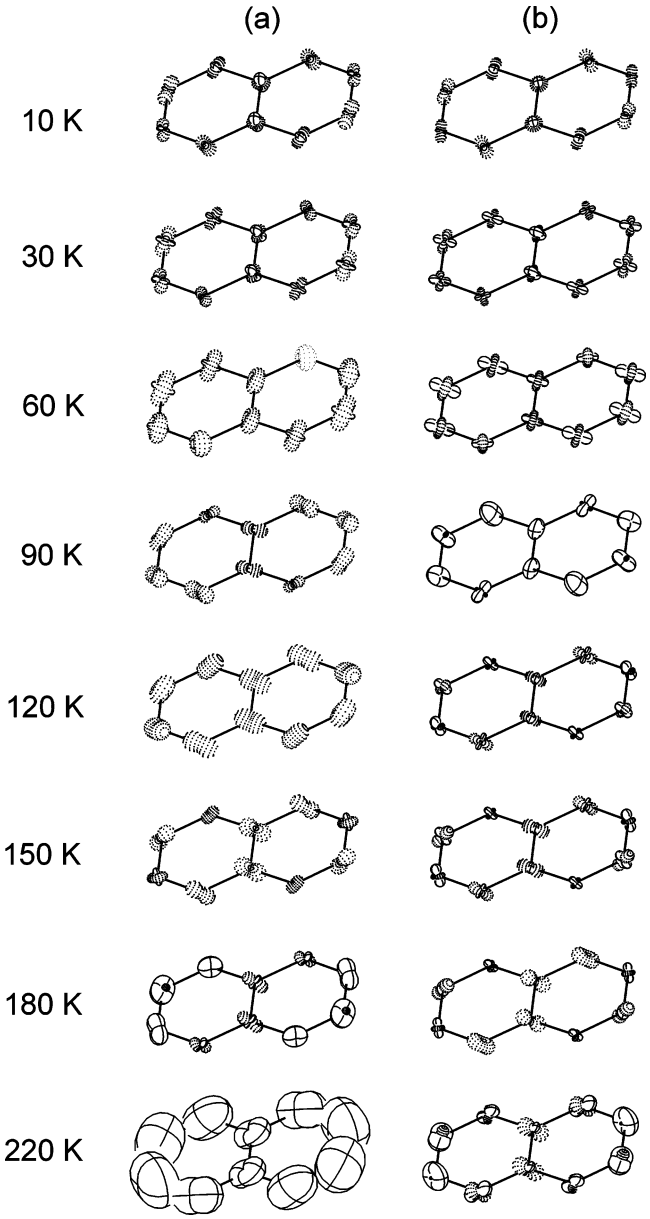

Figure 2. PEANUT plots[60] of the difference displacement parameters $U_{obs} - U_{calc}$ for naphthalene synchrotron data (see Table 1). (a) Schomaker and Trueblood TLS model; (b) anharmonic TLS,ϵ,γ model. Solid lines indicate positive differences, dotted lines indicate negative differences.

the experimental values of C_P measured by Southard and Brickwedde[63] in 1933 and by Chirico et al. more recently.[64]

In the temperature range 15−100 K, calculated values are higher than experimental ones. This is due to the Einstein approximation used in the ADP analysis, which neglects the linear dependence of the acoustic phonons on the wave vector in the inner part of the Brillouin zone.[5] In the temperature range 100−350 K, the calculated curve is lower than the experimental one. This discrepancy is probably associated with the anharmonic contribution to C_P:[65]

$$\Delta C_P = \frac{\chi^2 \cdot T \cdot V \cdot N_A}{2 \cdot \kappa_0} \qquad (6)$$

where V is the molar volume, χ the volume expansion coefficient, and κ_0 the compressibility of the crystal at zero pressure. [The volume has been expressed as $V = V_0 + a_2T^2 + a_3T^3$, and so the thermal expansion coefficient χ, i.e., the derivative of the volume as a function of temperature, takes the form: $\delta V/\delta T = \chi = 2a_2T + 3a_3T^2$. Note that the 2 in the denominator of eq 6 accounts for the two molecules in the unit cell.] The values of compressibility estimated from the difference between the calculated and experimental curves in the temperature range 100−300 K are compared in Table 5 with the literature values found for naphthalene[66,67] and with those calculated from temperature and pressure-dependence of the lattice parameters in d_8-naphthalene.[68,69]

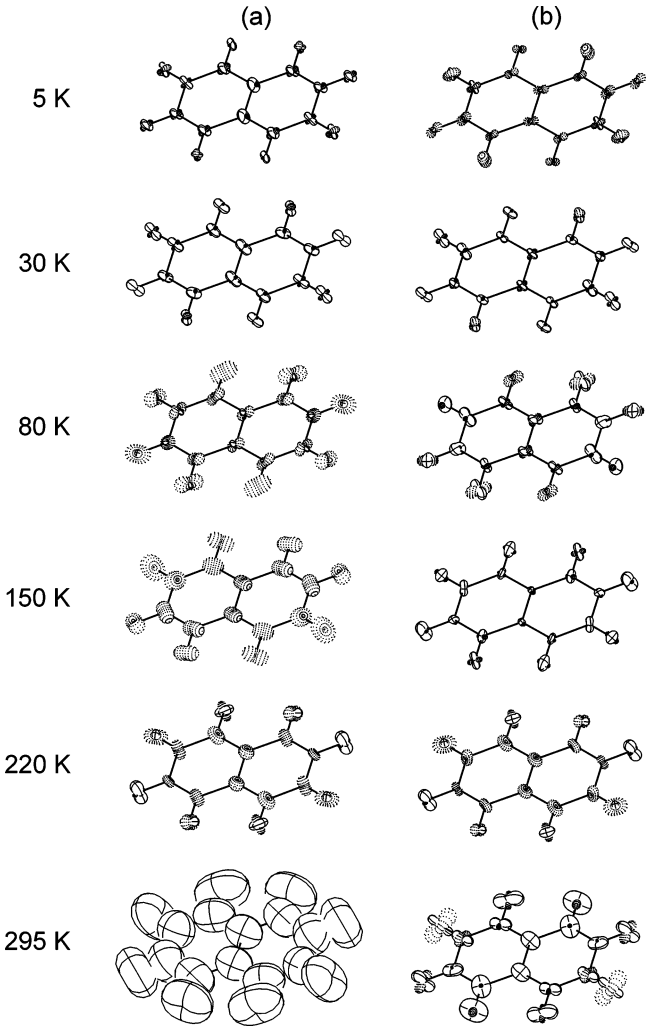

Figure 3. PEANUT plots[60] of the difference displacement parameters $U_{obs} - U_{calc}$ for naphthalene neutron data (see Table 3). (a) Schomaker & Trueblood TLS,ϵ1 model corrected for hydrogen internal motion; (b) anharmonic TLS,ϵ,γ model. Solid lines indicate positive differences, dotted lines indicate negative differences.

Conclusions

In this work, we have shown that the analysis of the temperature dependence of the ADPs provides a good description of the essential features of the molecular motion of the naphthalene molecule in the crystal. The frequencies and eigenvectors of the external normal modes, together with the contribution to the ADPs coming from the internal normal modes and a Grüneisen parameter to account for anharmonicity, have been refined from both synchrotron X-ray and neutron diffraction data and gave results comparable to those obtained by other experimental techniques. The increasing complexity of the model of motion gives clear indications that a simple rigid-body description is not sufficient to explain all the features

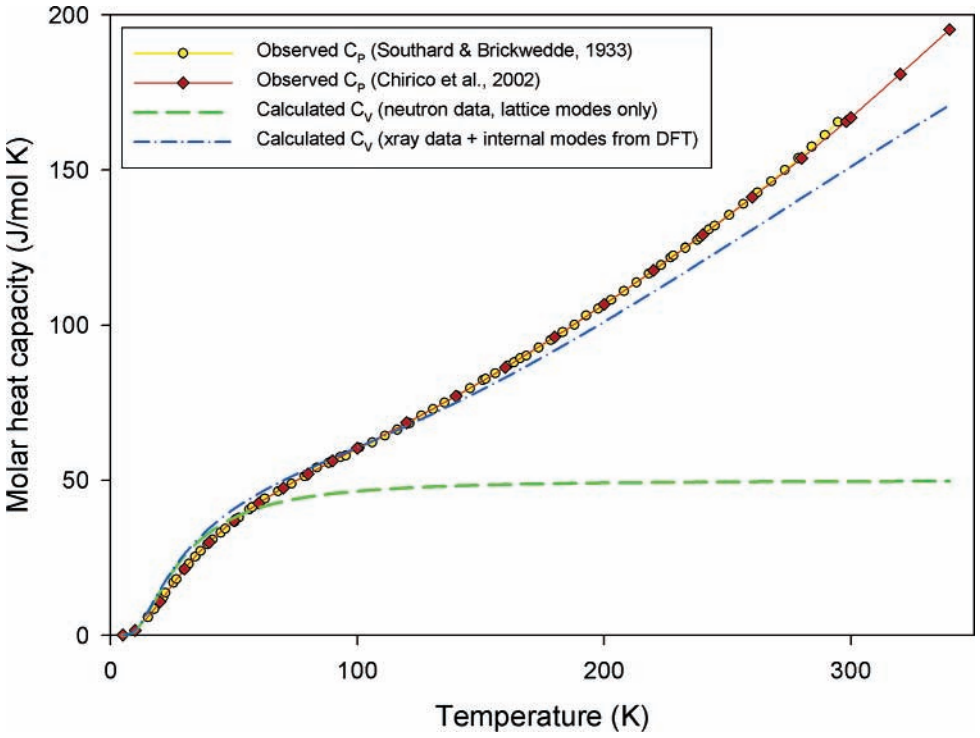

Figure 4. Molar heat capacity of naphthalene. Comparison of experimental and calculated values.

TABLE 5: Compressibility Values for Naphthalene in the Solid at 298 K (GPa^{-1})

data	experimental volume (diffraction data, Å^3)	calculated volume at 298 K (Å^3)	κ_0 internal freq. from DFT[46]	κ_0 internal freq. from SQM[26]	κ_0 internal freq. from DFT[26]	κ_0 exp.[66]	κ_0 exp.[67]	$\kappa_0{}^c$ calc.[68]	$\kappa_0{}^c$ calc.[69]
neutron	362.07 (at 295 K)	362.35	0.1897	0.1910	0.2088	0.185	0.173[d]	0.15	0.154
X-rays[a]	357.73 (at 280 K[b]	360.34	0.1902	0.1914	0.2091				

[a] Synchrotron data measured at ID11, ESRF, Grenoble; quadratic and cubic expansion coefficients from neutron volume expansion data. [b] Cell parameters from synchrotron powder data measured at ID11, ESRF, Grenoble (unpublished). [c] Data refers to d_8-naphthalene. [d] Best fit to pressure−volume data using the modified Murnaghan equation.

in the ADPs at multiple-temperatures, but including a simple ϵ tensor to account for the temperature-independent contributions to the ADPs leads to an improved fit of the observations. The addition of a single Grüneisen parameter to account for anharmonicity improves the analysis even further.

As already stated by Pawley and Cyvin,[49] naphthalene is a molecule for which we could expect the approximation of the separation between internal and external normal modes would not hold because of the closeness of the highest external to the two lowest internal mode frequencies, respectively 141 cm^{-1} at 2 K[21] and 176 and 193 cm^{-1} at 4.7 K.[28] Our model of motion could be extended to explicitly include the two lowest out-of-plane deformations, but we preferred to concentrate on the simplest models using the smallest possible number of parameters.

The method of ADP-analysis used in this work is easy to apply whenever multi-temperature diffraction data are available and allows a much better parameters-to-observable ratio than the usual Schomaker and Trueblood TLS analysis at a single temperature. For example: in this work, we have used a maximum of 19 parameters to describe all the 240 independent ADPs coming from the 8 synchrotron diffraction datasets and a maximum of 25 parameters for the 324 independent observations of the 6 neutron diffraction datasets, whereas with the usual TLS analysis we would need 12 parameters to fit 30 or 54 independent observations respectively from X-ray or neutron data.

Finally, the study of molecular motion in the solid state can be pursued by using a lattice dynamical approach, which has been successfully applied to small and medium-size organic molecules[38,39,50,70−72] or minerals.[73] Lattice dynamics, of course, offers a more complete treatment but the complexity of the calculation increases rapidly with the size of both the molecule and the lattice parameters. The ADP approach, on the other hand, also allows the analysis of part of the same structure independently of the rest, as (for example) in the study if the hydroquinone molecule in the $C_{60}(HQ)_3$ clathrate complex[74] or the dihydrogen ligands in the complex $Ru(H_2)(\eta^2\text{-}H_2)_2(Pcyp_3)_2$.[75] Furthermore, it has been shown for the benzene molecule that ADP-analysis and lattice dynamical calculations produce results in close agreement with one another.[76]

Acknowledgment. We are deeply indebted to Professor D. W. J. Cruickshank and Professor H. B. Bürgi for discussions of this work and to Professor S. Larsen for allowing access to her results before publication. The neutron data were collected at the Institut Laue Langevin in Grenoble, where excellent support was provided by the resident staff over an exceptionally long experimental period. The synchrotron data were collected at the ID11 Beamline of the ESRF in Grenoble during in-house research time.

References and Notes

(1) Cruickshank, D. W. J. *Acta Crystallogr.* **1956**, *9*, 754−756.
(2) Cruickshank, D. W. J. *Acta Crystallogr.* **1956**, *9*, 1005−1009.

(3) Cruickshank, D. W. J. *Acta Crystallogr.* **1956**, *9*, 1010−1011.
(4) Schomaker, V.; Trueblood, K. N. *Acta Crystallogr.* **1968**, *B24*, 63−76.
(5) Bürgi, H. B.; Capelli, S. C. *Acta Crystallogr.* **2000**, *A56*, 403−412.
(6) Grüneisen, E. *Ann. Phys.* **1912**, *39*, 257.
(7) Pawley, G. S.; Yeats, E. A. *Acta Crystallogr.* **1969**, *B25*, 2009−2013.
(8) Brock, C. P.; Dunitz, J. D. *Acta Crystallogr.* **1982**, *B38*, 2218−2228.
(9) Baharie, E.; Pawley, G. S. *Acta Crystallogr.* **1982**, *A38*, 803−810.
(10) Bürgi, H. B.; Rangavittal, N.; Hauser, J. *Helv. Chim. Acta* **2001**, *84*, 1889−1906.
(11) Oddershede, J.; Larsen, S. *J. Phys. Chem. A* **2004**, *108*, 1057−1063.
(12) Kastler, A.; Rousset, A. *J. Phys. Radium* **1941**, *2*, 49−57.
(13) Pimentel, G. C.; McClellan, A. L. *J. Chem. Phys.* **1952**, *20*(2), 270−277.
(14) Lippincott, E. R.; O'Reilly, E. J., Jr. *J. Chem. Phys.* **1955**, *23*(2), 238−244.
(15) McClellan, A. L.; Pimentel, G. C. *J. Phys. Chem.* **1955**, *23*(2), 245−248.
(16) Harada, I.; Shimanouchi, T. *J. Chem. Phys*. **1966**, *44*(5), 2016−2028.
(17) Suzuki, M.; Yokoyama, T.; Ito, M. *Spectrochim. Acta* **1968**, *22A*, 1091−1107.
(18) Wyncke, B.; Hadni, A. *Comptes Rendus Acad. Sc. Paris* **1972**, *275 B*, 825−828.
(19) Wu, C. K.; Nicol, M. *J. Chem. Phys.* **1973**, *58*(11), 5150−5162.
(20) Hineno, M.; Yosinaga, H. *Spectrochim. Acta* **1974**, *31A*, 617−620.
(21) Bellows, J. C.; Prasad, P. N. *J. Chem. Phys.* **1979**, *70*(4), 1864−1871.
(22) Chronister, E. L.; Hill, J. R.; Dlott, D. D. *J. Chim. Phys. (Paris)* **1985**, *82*(2−3), 159−168.
(23) Sellers, H.; Pulay, P.; Boggs, J. E. *J. Am. Chem. Soc.* **1985**, *107*, 6487−6494.
(24) Häfner, W.; Kiefer, W. *J. Chem. Phys.* **1986**, *86*(8), 4582−4596.
(25) Hudgins, D. M.; Sandford, S. A.; Allamandola, L. J. *J. Phys. Chem.* **1994**, *98*, 4243−4253.
(26) Cané, E.; Palmieri, P.; Tarroni, R.; Trombetti, A.; Handy, N. C. *Gazz. Chim. It.* **1996**, *126*, 289−296.
(27) Han, J.; Xu, H.; Zhu, Z.; Yu, X.; Li, W. *Chem. Phys. Lett.* **2004**, *392*, 348−351.
(28) Bokhenkov, E. L.; Natkaniec, I.; Sheka, E. F. *Phys. Status Solidi B* **1976**, *75*, 105−116.
(29) Bokhenkov, E. L.; Sheka, E. F.; Dorner, B.; Natkaniec, I. *Solid State Commun.* **1977**, *23*, 89−93.
(30) Bokhenkov, E. L. *Annex Ann. Report ILL*, 1976.
(31) Bokhenkov, E. L.; Rodina, E. M.; Sheka, E. F.; Natkaniec, I. *Phys. Stat. Sol. (b)* **1978**, *85*, 331−342.
(32) Natkaniec, I.; Bokhenkov, E. L.; Dorner, B.; Kalus, J.; Mackenzie, G. A.; Pawley, G. S.; Schmelzer, U.; Sheka, E. F. *J. Phys. C*: *Solid State Phys.* **1980**, *13*, 4265−4283.
(33) Dorner, B.; Bokhenkov, E. L.; Sheka, E. F.; Chaplot, S. L.; Pawley, G. S.; Kalus, J.; Schmelzer, U.; Natkaniec, I. *J. Phys. (Paris)* **1981**, *C6*, 602−604.
(34) Schmelzer, U.; Bokhenkov, E. L.; Dorner, B.; Kalus, J.; Mackenzie, G. A.; Natkaniec, I.; Pawley, G. S.; Sheka, E. F. *J. Phys. C*: *Solid State Phys.* **1981**, *14*, 1025−1041.
(35) Kalus, J.; Dorner, B.; Jindal, V. K.; Karl, N.; Natkaniec, I.; Pawley, G. S.; Press: W.; Sheka, E. F. *J. Phys. C: Solid State Phys.* **1982**, *15*, 6533−6544.
(36) Sheka, E. F.; Bokhenkov, E. L.; Dorner, B.; Kalus, J.; Mackenzie, G. A.; Natkaniec, I.; Pawley, G. S.; Schmelzer, U. *J. Phys. C*: *Solid State Phys.* **1984**, *17*, 5893−5914.
(37) Pawley, G. S. *Phys. Status Solidi* **1969**, *20*, 347−360.
(38) Filippini, G.; Gramaccioli, C. M.; Simonetta, M.; Suffritti, G. B. *J. Chem. Phys.* **1973**, *59*(9), 5088−5101.
(39) Gramaccioli, C. M.; Filippini, G.; Simonetta, M. *Acta Crystallogr.* **1982**, *A38*, 350−356.
(40) Criado, A. *Acta Crystallogr.* **1989**, *A45*, 409−415.
(41) Della Valle, R. G.; Fracassi, P. F.; Righini, R.; Califano, S. *Chem. Phys.* **1983**, *74*, 179−195.
(42) Della Valle, R. G.; Pawley, G. S. *Acta Crystallogr.* **1984**, *A40*, 297−305.
(43) Pawley, G. S. *Solid State Commun.* **1985**, *53*, 817−821.
(44) Swiderek, P.; Hohlneicher, G.; Maluendes, S. A.; Dupuis, M. *J. Chem. Phys.* **1993**, *98*(2), 974−987.
(45) Langhoff, S. R. *J. Phys. Chem.* **1996**, *100*, 2819−2841.
(46) Martin, J. M.; El-Yazal, J.; Francois, J. P. *J. Phys. Chem.* **1996**, *100*, 15358−15367.
(47) Bauschlicher, C. W., Jr.; Langhoff, S. R.; Sandford, S. A.; Hudgins, D. M. *J. Phys. Chem.* **1997**, *101*, 2414−2422.
(48) Lokshin, B. V.; Borisova, N. E.; Senyavin, B. M.; Reshetova, M. D. *Russ. Chem. Bull. Int. Ed.* **2002**, *51*(9), 1656−1666.
(49) Pawley, G. S.; Cyvin, S. J. *J. Chem. Phys.* **1970**, *52(8)*, 4073−4077.
(50) Gramaccioli, C. M.; Filippini, G. *Acta Crystallogr.* **1983**, *A39*, 784−791.
(51) Della Valle, R. G.; Venuti, E.; Brillante, A. *Chem. Phys.* **1995**, *198*, 79−89.
(52) Jindal, V. K.; Dlott, D. D. *J. Appl. Phys.* **1998**, *83*(10), 5203−5211.
(53) Dows, D. A.; Hsu, L.; Mitra, S. S.; Brafman, O.; Hayek, M.; Daniels, W. B.; Crawford, R. K. *Chem. Phys. Lett.* **1973**, *22*(3), 595−599.
(54) Nicol, M.; Vernon, M.; Tak Woo, J. *J. Chem. Phys.* **1975**, *63*(5), 1992−1999.
(55) Bruker Software: *SMART*(Version 5.618), *SAINT*(Version 6.41A), and *SADABS*(Version 2.05); Bruker AXS Inc.: Madison, Wisconsin, 2000.
(56) Sheldrick, G. M. *SHELXL97*, Release 97−2; Program for the Refinement of Crystal Structures: University of Göttingen, Germany, 1997.
(57) Burnett, M. N.; Johnson, C. K. *ORTEP−III − Oak Ridge Thermal Ellipsoid Plotting Program for Crystal Structure Illustrations*, ORNL-6895; Oak Ridge National Laboratory, 1996.
(58) Bürgi, H. B.; Förtsch, M.; Capelli, S. C.; Hauser, J. *NKA: Program for Normal Coordinate Analysis from Anisotropic Displacement Parameters at Multiple Temperatures*, Version 5.1.17; University of Bern, Switzerland, 2004.
(59) Bürgi, H. B.; Capelli, S. C.; Birkedal, H. *Acta Crystallogr.* **2000**, *A56*, 425−435.
(60) Hummel, W.; Hauser, J.; Bürgi, H. B. *J. Mol. Graphics* **1990**, *8*, 214−220.
(61) Andrews, F. C. *Equilibrium Statistical Mechanics*; John Wiley & Sons: London, 1963.
(62) Raif, F. *Fundamentals of Statistical and Thermal Physics*; McGraw-Hill: Singapore, 1965; pp 253−256.
(63) Southard, J. C.; Brickwedde, F. G. *J. Am. Chem. Soc.* **1933**, *55*, 4378−4384.
(64) Chirico, R. D.; Knipmeyer, S. E.; Steele, W. V. *J. Chem. Thermodyn.* **2002**, *34*, 1873−1884.
(65) Guggenheim, E. A. *Thermodynamics*, 5th ed.; North-Holland Physics Publishing: Amsterdam, 1967; p 89.
(66) Adams, L. H. In *International Critical Tables*; McGraw-Hill: New York, 1928; Vol. III, p 49.
(67) Vaidya, S. N.; Kennedy, G. C. *J. Chem. Phys.* **1971**, *55*(3), 987−992.
(68) El Hamamsy, M.; Elnahwy, S.; Damask, A. C.; Taub, H.; Daniels, W. B. *J. Chem. Phys.* **1977**, *67*(2), 5501−5504.
(69) Jordan, J. F. J.; Axmann, A.; Egger, H.; Kalus, J. *Phys. Status Solidi A* **1982**, *71*, 457−462.
(70) Filippini, G.; Gramaccioli, C. M. *Acta Crystallogr.* **1989**, *A45*, 261−263.
(71) Filippini, G.; Gramaccioli, C. M. *Acta Crystallogr.* **1986**, *B42*, 605−609.
(72) Gramaccioli, C. M.; Filippini, G. *Acta Crystallogr.* **1985**, *A41*, 361−365.
(73) Gramaccioli, C. M., Ed. *Energy Modelling in Minerals*; EMU Notes in Mineralogy, Vol. 4; 4th EMU School of Mineralogy: Budapest, 2002.
(74) Bürgi, H. B.; Capelli S. C. *Helv. Chim. Acta* **2003**, *86*, 1625−1640.
(75) Albinati, A.; Capelli, S. C.; Mason, S. A. Unpublished.
(76) Capelli, S. C.; Förtsch, M.; Bürgi, H. B. *Acta Crystallogr.* **2000**, *A56*, 413−424.
(77) Full listing of crystal lattice parameters, coordinates, anisotropic displacement parameters, bond distances, bond angles, and torsion angles in CIF format has been deposited with the Cambridge Crystallographic Data Centre (deposition numbers: *600174−600187*). These data can be obtained free of charge via http://www.ccdc.cam.ac.uk/data_request/cif, or by e-mailing data_request@ccdc.cam.ac.uk, or by contacting The Cambridge Crystallographic Data Centre, 12, Union Road, Cambridge CB2 1EZ, UK; fax: +44 1223 336033.